Journal of Power Sources 506 (2021) 230039

Contents lists available at ScienceDirect

Journal of Power Sources

journal homepage: www.elsevier.com/locate/jpowsour

Development of high-performance roll-to-roll-coated gas-diffusion-electrode-based fuel cells

Scott A. Mauger [a,*], Min Wang [a,1], Firat C. Cetinbas [b], Michael J. Dzara [c], Jaehyung Park [d], Deborah J. Myers [d], Rajesh K. Ahluwalia [b], Svitlana Pylypenko [c], Leiming Hu [e,2], Shawn Litster [e], K.C. Neyerlin [a], Michael Ulsh [a]

[a] Chemistry and Nanoscience Center, National Renewable Energy Laboratory, Golden, CO, 80401, USA
[b] Energy Systems Division, Argonne National Laboratory, Lemont, IL, 60439, USA
[c] Department of Chemistry, Colorado School of Mines, Golden, CO, 80401, USA
[d] Chemical Sciences and Engineering Division, Argonne National Laboratory, Lemont, IL, 60439, USA
[e] Department of Mechanical Engineering, Carnegie Mellon University, Pittsburgh, PA, 15213, USA

HIGHLIGHTS

- Method to make high-performance roll-to-roll coated GDEs developed.
- Rapid drying of catalyst layer found to enrich ionomer at top surface.
- Ionomer-rich catalyst layer surface forms low-resistance interface with membrane.
- Roll-to-roll coated GDEs perform as well as spray-coated GDEs.

ARTICLE INFO

Keywords:
PEM fuel Cells
Roll-to-roll coating
Gas diffusion electrodes
Slot die coating

ABSTRACT

This study focuses on determining fabrication conditions to create high-performance roll-to-roll-coated (R2R-coated) gas-diffusion electrodes (GDEs) for proton-exchange-membrane fuel cells (PEMFCs). Here, we examine how process conditions influence the distribution of ionomer in the electrode, which is shown to be critical for high performance. Using a combination of Kelvin probe, X-ray photoelectron spectroscopy, and nano-scale X-ray computed tomography we show that formation of an ionomer-rich surface is promoted by using a higher drying rate. We show that R2R-coated GDEs have higher surface ionomer concentration than spray-coated GDEs, which enables these R2R-coated GDEs to not need an additional ionomer overlayer, as is typically the case for spray-coated GDEs. This will reduce the number of processing steps and lower material costs in a manufacturing setting. This work shows that with the appropriate selection of materials, ink formulation, and processing conditions, direct-coated GDEs are a viable pathway for fuel cell manufacturing.

1. Introduction

The challenge for any energy technology to advance from the laboratory to a product is the ability to translate the high performance of laboratory scale to mass production. Scale-up can present challenges for both materials synthesis and device fabrication. For PEMFCs, fabrication of the membrane-electrode assembly (MEA) presents challenges for mass production. Specifically, to meet the production volumes needed for widespread use of fuel-cell electric vehicles, continuous roll-to-roll (R2R) processes will be needed [1]. Therefore it is critical to determine pathways for high-performance MEAs fabricated using R2R processes.

The catalyst layers of an MEA are typically fabricated through two pathways: direct coating or decal transfer. In direct coating, the catalyst layer is coated directly onto the membrane or gas diffusion media. In the decal transfer process, the catalyst layer is coated to a decal substrate

* Corresponding author.
E-mail address: scott.mauger@nrel.gov (S.A. Mauger).
[1] Current address: Southern University of Science and Technology, Shenzhen, Guangdong Province 518055, China.
[2] Current address: Chemistry and Nanoscience Center, National Renewable Energy Laboratory, Golden, CO, 80401, USA.

https://doi.org/10.1016/j.jpowsour.2021.230039
Received 20 October 2020; Received in revised form 11 May 2021; Accepted 12 May 2021
Available online 7 June 2021
0378-7753/© 2021 Elsevier B.V. All rights reserved.

(sometimes referred to as a transfer liner) and then laminated to the membrane in a hot-pressing transfer step. For mass production, direct coating is advantageous as it reduces both process and materials costs. Manufacturing cost analysis has shown that at a production volume of 500,000 light-duty vehicle stacks per year, the decal substrate and the transfer process together cost approximately 1.67 times the cost of the electrode coating process itself [2,3]. In addition, this analysis does not account for the cost associated with incomplete transfer of the expensive catalyst and ionomer materials to the membrane during the transfer process. Thus, there is a need to develop coating processes and device constructions that are amenable to high-volume direct coating, while also achieving the high performance of laboratory-scale MEAs.

In direct coating, the catalyst layer can be applied directly to the membrane to form a catalyst-coated membrane (CCM). CCMs generally produce high-performance MEAs due to a low contact resistance at the catalyst layer – membrane interface [4]. However, perfluorosulfonic acid (PFSA) membranes are prone to swelling in the catalyst ink dispersion media. For lab-scale processes this can be easily overcome by mechanically stabilizing the membrane on a vacuum table during coating of the catalyst layer. However, this approach is likely impractical in continuous R2R processes. Researchers have developed other strategies for direct coating of membranes such as pre-swelling the membrane [5,6] or choosing a solvent system to minimize membrane swelling [7]. However, these approaches have not been adapted for R2R processing, likely because they require additional process steps or use dispersion media with very high boiling points. As a result, many manufacturers use the decal transfer process to fabricate CCMs as coating on a decal substrate and the transfer process do not present logistical challenges for R2R processing [8,9].

Alternately, gas-diffusion electrodes (GDEs) can be fabricated by coating the catalyst onto the microporous layer (MPL) of the gas diffusion media. Relative to membranes, gas diffusion media (GDM) is a more amenable substrate for direct coating, since it does not swell when in contact with the catalyst ink. There may also be performance advantages to GDEs. GDEs have lower thermal and electronic resistances than CCMs, the latter of which reduces MEA high-frequency resistance [10,11]. Also, water pooling at the catalyst layer – MPL interface has been shown to limit reactant transport in CCMs [12,13]. Thus the more integral catalyst layer – MPL interface expected in GDEs is likely to improve reactant transport.

Despite these advantages, the performance of GDE-based MEAs has often lagged behind that of CCM-based MEAs due to a poor catalyst layer – membrane interface [4]. Several researchers have sought to improve GDE-based MEAs by coating a layer of ionomer on top of the catalyst layer prior to interfacing it with the membrane. Despite the improvements observed, the GDE-based MEAs still did not match the performance of CCM-based MEAs [14–17]. Recently, we demonstrated that spray-coated GDE-based MEAs could match the performance of CCM-based MEAs by using a thin ionomer overlayer and subsequently hot pressing the GDE to the membrane [18]. In a follow up study, we showed that decreasing the MPL roughness reduced the required ionomer overlayer thickness for maximum performance, highlighting the need to select materials appropriately for MEA construction [19]. However, for mass production this two-layer construction (catalyst layer plus ionomer overlayer) does not present much of an advantage over a R2R decal transfer process as both involve two process steps. Therefore, it is desirable to develop a single-step R2R process, i.e., one coating step only, to produce high performance GDEs.

Based on our studies of spray-coated GDEs and ionomer overlayers we hypothesized that a R2R-coated GDE with a naturally-occurring high concentration of ionomer at the top surface would remove the need for an additional ionomer overlayer. To that end, it has been previously established that in the drying of mixtures of colloidal particles, such as fuel cell catalyst inks, the distribution of particles is impacted by factors such as the drying rate, particle size, and concentration [20–25]. We suspected that in R2R-coated catalyst layers, through appropriate selection of ionomer-to-carbon (I/C) ratio and drying parameters, a catalyst layer with an ionomer-rich top (membrane-facing) surface could be prepared in a single coating step. We expected that at high ionomer concentrations, not all of the ionomer would be adsorbed on the catalyst or support and therefore be free to segregate to the top surface of the catalyst layer. This structure would mimic the bilayer structure created by spraying an ionomer overlayer onto the catalyst layer, and minimize the contact resistance between the catalyst layer and the membrane, removing the need for an ionomer overlayer produced with an additional coating step.

From prior theoretical and experimental studies, a consistent understanding has been established for colloidal dispersions, which can be applied to fuel cell catalyst inks. When a film consolidates, there are three forces that dictate the distribution of materials – evaporation, diffusion, and sedimentation [21]. The relative importance of these forces can be assessed using the dimensionless Peclet (*Pe*) and sedimentation (N_s) numbers. *Pe* characterizes the importance of evaporation relative to diffusion and is defined as,

$$Pe = \frac{EH_0}{D_0} \tag{1}$$

where E is the velocity of the free surface moving towards the substrate, H_0 is the initial thickness of the wet film, and D_0 is the Stokes-Einstein diffusion coefficient. A high *Pe* indicates the consolidation process is evaporation dominated. In Equation (2), N_s characterizes the importance of evaporation relative to sedimentation:

$$N_s = \frac{U_0}{E} \tag{2}$$

where U_0 is the sedimentation velocity of the particles. For the majority of conditions, U_0 is small relative to E and D_0, thus N_s is low, meaning evaporation and diffusion are the primary competing forces [21,26]. Previous studies have found that for dispersions with two sizes of colloidal particles, high *Pe* leads to stratification in the final dried film with the surface rich in the smaller particles [20,22,23,27]. In these conditions the larger particles are pinned at the rapidly descending drying front. Capillary forces drive the smaller particles through the interstitial voids between the large particles and displace them at the surface creating a surface rich in the smaller particles. In the case of high solids volume fraction and a small difference in size between the two types of particles, the stratification is less pronounced and there tends to be more of a gradual increase in small particles towards surface rather than a fully stratified small particle layer [20]. At low *Pe,* Brownian diffusion counteracts capillary forces and particles at the surface diffuse back towards the bulk of the film resulting in a more homogenous distribution of materials. Based on this understanding we would expect that increasing the drying temperature, thus increasing *Pe*, would promote enrichment of ionomer at the top surface. However, ionomer adsorbs on to the Pt/C surface, which may limit its ability segregate. Thus, an exploration of how ink formulation and drying impact the ionomer distribution throughout the of the catalyst layer is needed.

In this work, we investigated the impact of drying temperature and ionomer concentration in the catalyst ink on the concentration of ionomer at the top surface of the GDE and the resulting impact on fuel cell performance. Using a combination of Kelvin probe and X-ray photoelectron spectroscopy (XPS) we show that by increasing the drying temperature and ionomer concentration we are able to increase the ionomer content at the top surface of the catalyst layer. This enables the production of R2R-coated GDEs, coated in a single step with a single ink, that have the same, if not slightly higher, performance than two-step spray-coated GDEs with an overlayer. Overall, this work shows that GDEs are a promising option for mass production of MEAs.

2. Materials and methods

Materials – The catalyst used in this study was a 46 wt% Pt on high surface area carbon (Pt/HSC, Tanaka TEC10E50E). The ionomer dispersion was a 20 wt% dispersion of Nafion™ (1000 EW) in a mixture of water and 1-propanol (D2020, Ion Power). For all MEAs, 25 μm thick Nafion™ membranes (NR-211, Ion Power) were used. Two diffusion media were used: Sigracet 29 BC (SGL Carbon) and H23C8 (Freudenberg).

Spray Coating – Spray-coated catalyst layers were prepared using dilute catalyst inks and an ionomer dispersion. The catalyst ink and ionomer dispersion were prepared with the same formulation and procedure as we have previously used to prepare GDEs [18,19]. Briefly the catalyst powder was weighed into a glass jar followed by the addition of deionized water, gentle swirling, 1-propanol, and the ionomer dispersion. The I/C of the catalyst ink was 0.9 I/C. The ink was mixed using a combination of tip and bath ultrasonication.

Spray coating was used to prepare GDE and CCM catalyst layers, as we have previously reported [18,19]. The inks were spray coated using a 25 kHz Accumist nozzle on a SonoTek ultrasonic spray coating station. For the catalyst layers, the volumetric flow rate was 0.3 mL/min. The catalyst layer loading was 0.1 mg_{Pt}/cm^2. For the ionomer overlayer, the flow rate was 0.15 mL/min. The loading of the ionomer overlayer was 0.045 mg_{Nafion}/cm^2, as detailed in our previous publication [18].

Mayer Rod and Roll-to-Roll Coating – Inks for Mayer rod and R2R coating are more concentrated then those used for spray coating. The inks were prepared by weighing the catalyst powder into a glass jar, adding the required amounts of deionized water, followed by 1-propanol, and then ionomer dispersion. The inks were mixed using a high-shear disperser (T25 Ultra Turrax, IKA) for 15 min at 10,000 rpm. The water/1-propanol ratio of the final inks was 75/25 by weight. The Pt/HSC content in these inks was 3.2 wt%. The mass of ionomer dispersion added to the ink was varied to achieve the desired I/C ratio.

Small-scale GDEs were prepared using Mayer rod coating. This process simulates R2R coating as a single film is used to create the catalyst layer. The rods were drawn by hand. After coating, these samples were dried in the air flotation oven of the R2R coating line.

For R2R-coated samples, catalyst layers were coated using slot die coating on a Yasui Seki - MIRWEC Mini-Labo Deluxe coating station, as shown in Fig. 1a. A slot die (Premier Dies) with a slot gap of 250 μm and a coating width of 8 cm was used. The die was mounted horizontally, and the coating was performed with a backing roller, as shown in Fig. 1b. The web speed was 1 m/min. The gap between the die lip and substrate was varied for each ink in order to obtain a stable coating bead. The coatings were dried in the air flotation ovens of the coating line at 80 °C.

Loading Characterization – The Pt loadings of the GDE electrodes were measured using X-ray fluorescence spectroscopy (XRF) (Fischerscope XDV-SDD, 50 kV, 50 W X-ray source). The instrument calculates the Pt loading from the measured spectrum using a fundamental parameters approach. This is based on physical models for all the aspects of the XRF experiment, such as absorption, enhancement, specimen geometry, fluorescence yield, and spectral output. For each GDE the loading was measured at 5 locations to characterize the average loading. For all electrodes the Pt loading varied by less than 5% across the electrode. For electrodes of the same Pt loading the variation between electrodes was also less than 5%.

MEA Assembly – The MEAs used GDEs as cathodes. Anodes with a 0.1 mg_{Pt}/cm^2 loading were prepared by direct spray coating onto the membrane to create a half-CCM prior to full MEA assembly. The full MEAs were assembled by hot pressing the GDE cathode to the anode-half-CCM along with the anode gas diffusion layer (GDL), which was the same as the cathode GDL. The MEAs were hot pressed for 3 min at 125 °C between Kapton and Gylon sheets and stainless steel plates, as previously described [18]. The total applied force was 25 kg/cm^2_{gylon}. The stacks were removed from the press and allowed to cool to near room temperature. Then the MEAs were removed from the plates and polymer sheets. The MEA active area was 50 cm^2.

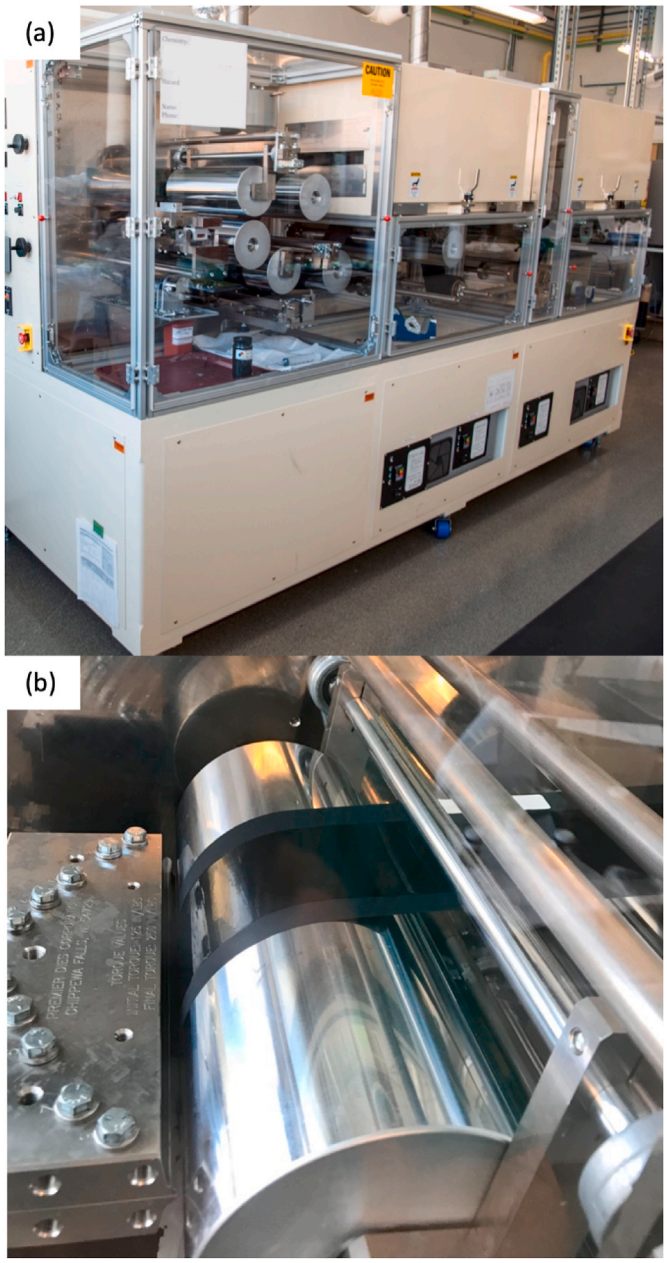


Fig. 1. Photographs of the (a) roll-to-roll coating station and (b) slot die coating the catalyst layer on gas diffusion media.

MEA Testing – The MEAs were tested in single-cell hardware with graphite flow fields with double/triple serpentine (anode/cathode) patterns. The MEAs were sealed between polytetrafluoroethylene (PTFE) gaskets. The thicknesses of the gaskets were measured and appropriate thicknesses were selected to compress the diffusion media to 82% of its original thickness, based on the manufacturer's recommendations. All MEAs were conditioned the same procedure. This procedure consisted of a break-in procedure of voltage cycling. This was followed by cycles of holding at 0.1 V followed by polarization curves [28,29]. The reported polarization curves were measured following the third conditioning cycle. Our prior work has shown the mass activity plateaus after three cycles for this catalyst/membrane system [29]. Polarization curves were measured with an anodic sweep direction. The reported current density/voltage is the average value measured in the minute following a 3 min equilibration period. Oxygen polarization curves were

measured using voltage-control mode. Air polarization curves were measured using current-control mode. The anode and cathode stoichiometries were 1.5 and 2, respectively. Polarization curves were measured under conditions of 80 °C, 150 kPa absolute and 100% RH (O_2 and air).

Cyclic voltammograms (CVs) were measured at 30 °C, 150 kPa total cell pressure, 100% RH, with H_2 on the anode and N_2 on the cathode at flow rates of 0.50 and 0.05 slpm, respectively. The CVs were recorded from 0.05 to 1.2 V at a sweep rate of 50 mV/s using an Autolab PGSTAT302 N potentiostat (MetrOhm AG). The electrochemically-active surface area (ECSA) was determined from the integrated area of the hydrogen underpotential deposition (H_{UPD}) region (≈0.1–0.4 V) of the CVs [30,31].

Electrochemical impedance spectra were measured at 80 °C, 150 kPa absolute total cell pressure, 100% RH, and H_2 and N_2 flow rates of 0.2 slpm. The spectra consisted of 40 points from 1 Hz–10 kHz on a logarithmic scale. The DC voltage was 0.2 V and the AC perturbation voltage was 1 mV. The spectra were modeled using a physics-based modified-transmission-line model in an open-source custom-programed complex-valued non-linear least-squares fitting program [18,32,33].

Kelvin Probe – The contact potential difference (CPD) of the GDEs was measured using an ambient Kelvin probe with a gold-alloy tip (KP Technology, Ltd.), as previously described [34]. Proper function of the system was ensured by measuring reference samples of gold and aluminum with a native oxide. The measurement system was enclosed in a Faraday cage to minimize electrical noise in the system. The position of the tip was manually adjusted to set a gradient between the tip and sample in the range of 290–310 mV. The probe amplitude was 50 and the frequency was 78 Hz. The samples were grounded by contacting them with a metal needle. The reported CPD values are the average of 20 measurements.

Nano-scale X-ray Computed Tomography (nano-CT) – Prior to mounting the GDE samples on the tomography pins the GDE samples were soaked for 72 h in a saturated cesium sulfate solution (with solubility of 167 g/100 mL) to ion exchange the sulfonic acid groups of the ionomer with Cs^+ [35]. The ion-exchanged sample was rinsed with copious amounts of deionized water to remove excess salt and then dried at room temperature. As described below, Cs^+ exchange is necessary to visualize the ionomer by nano-CT. The dried GDE samples were then cut into ~0.5 mm x ~0.5 mm pieces using a scalpel and attached to the flat end of a pin using silver-epoxy composite adhesive. The electrodes were then laser-milled (QuickLaze 50ST2, ESI®) to form ≤50 μm diameter circular pillars. Samples of this size are needed for the nano-CT measurements such that the entire sample stays in the field of view of the nano-CT instrument during rotation.

X-ray radiographs were acquired using the Xradia nano XCT-S100 TXM at beam line 32-ID-C of the Advanced Photon Source (APS) at Argonne National Laboratory (ANL). Employing a fly-scan technique, 1080 projection images were acquired over 180° of rotation. Images were acquired in both absorption and Zernike phase contrast modes without removing the sample from the tomography stage. The phase contrast mode facilitates imaging low electron density materials and resolves the secondary pore morphology and the structure of the solid electrode (as a mixture of C, Pt, ionomer, and primary pores). The absorption contrast relies on differences in the electron density of the electrodes' constituents and shows the location of the electron-rich Cs^+-exchanged ionomer. Catalyst particles also contribute to the absorption-contrast images; however, the volume of the catalyst particles is small compared to the volume of the ionomer. The projection images were reconstructed into 3D image sequence with ~20-nm voxel size using Tomopy with Astra [36]. Nano-CT data was further quantified by segmenting the phase contrast image using open source Fiji software [37], as discussed in detail in Cetinbas et al. [38] The volume fraction of ionomer was determined based on the methods developed by Komini Babu et al. [35].

2.1. X-ray photoelectron spectroscopy

X-ray photoelectron spectroscopy (XPS) measurements were performed using a custom Scienta-Omicron HiPP-3 system equipped with a R4000 hemispherical analyzer operating in swift acceleration mode [39] calibrated to the Au 4f region of a sputter cleaned Au foil. An Al K_α X-ray source was operated with a 900 μm spot size at 300 W, and all core level measurements were performed at a combination of a 200 eV pass energy and a 0.8 mm × 30 mm slit size resulting in an estimated energy resolution of 0.59 eV. Analysis chamber pressure was maintained at a level below 5.0×10^{-8} mbar, while analyzer pressure remained below 1×10^{-8} mbar. Samples were mounted on conducting carbon tape and therefore no charge referencing was necessary. All C 1s spectra were acquired within 20 min of initially exposing the samples to the X-ray source to avoid any artifacts that may occur due to Nafion™ instability.

Spectral processing was performed using CasaXPS software, where a Shirley background was applied to the C 1s. Curve-fitting was performed using a least-squares method, featuring 8 components with a 30% Gaussian, 70% Lorentzian line shape. The binding energy (BE) position and full width at half-maximum (FWHM) values for each component were constrained to a range of 0.2 eV and 0.1 eV, respectively. A table of fitting parameters is supplied in Table S1 of the Supporting Information for all curve-fits displayed. Assignment of spectral components to chemical species is based upon both prior experience and relevant literature [40,41].

3. Results and discussion

To understand the factors that control the distribution of ionomer we started by preparing small-scale samples with different ink formulations using Mayer rod coating. For brevity, these will henceforth be referred to as "rod-coated". Since this coating method creates a thick wet film, the film consolidation is similar to what would occur in a continuous R2R process. Inks with three I/C ratios (0.9, 1.2, and 1.6) were coated on SGL 29BC diffusion media and dried at different temperatures. An I/C of 0.9 is thought to be near optimum for the high-surface-area support used here and is what we typically use for spray-coated GDEs [18,19,42]. We hypothesized that higher amounts of ionomer in the ink could lead to an increased surface concentration of ionomer, assuming the additional ionomer remains freely dispersed in the ink and does not adsorb on the catalyst or support. The catalyst layers were dried in the forced-air oven of the R2R coating system. Forced air has been shown to lead to more polymer at the surface than still air, thus these ovens should promote the formation of an ionomer rich surface [22]. The oven temperatures tested were 25, 60, and 80 °C.

Given that our ultimate goal was to determine if we could create an ionomer-rich catalyst layer surface, we initially characterized these samples using a Kelvin probe. A Kelvin probe measures the CPD between a sample surface and a reference metal tip. The CPD is the difference between the work function of the reference electrode tip and the surface potential of the measured sample. A sample's surface potential is determined, in part, by the chemical composition of the surface. For a surface containing multiple components, a Kelvin probe can provide qualitative assessment of the surface composition, provided there is significant contrast between the components [43]. We have previously shown that this method is able to distinguish between catalyst layers with different ionomer content [34].

Fig. 2 shows the measured CPDs for the rod-coated catalyst layers described above. Because CPD is a relative measurement, the values in the plot have been normalized by subtracting the measured CPD of a spray-coated-GDE catalyst layer without an ionomer overlayer from the measured CPD of the other samples. Therefore, CPD values greater than zero indicate a higher surface ionomer content than the spray-coated catalyst layer without an overlayer. Also included as a dashed line is the CPD value for a spray-coated catalyst layer with an ionomer overlayer. The top surface of the spray-coated GDE with ionomer overlayer

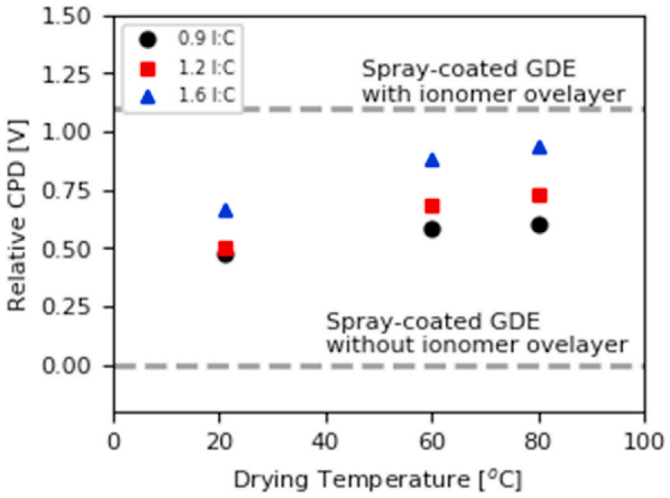


Fig. 2. Kelvin probe measurements of the relative contact potential difference (CPD) of rod-coated GDEs. Measured CPD values are calculated relative to the spray-coated GDE without an ionomer overlayer. Catalyst inks had I/C of 0.9 (black), 1.2 (red), or 1.6 (blue). (For interpretation of the references to colour in this figure legend, the reader is referred to the Web version of this article.)

has a high ionomer concentration, and therefore a high CPD. These two spray-coated samples provide a useful reference against which to qualitatively understand how I/C ratio and drying temperature influence the surface ionomer concentration of rod-coated samples.

There are several noteworthy observations from the CPD results for the rod-coated samples. First, all of the rod-coated catalyst layers have a higher CPD, and thus a higher surface ionomer content, than the spray-coated catalyst layer without an ionomer overlayer. This is even the case at 0.9 I/C, which is the same I/C as the spray-coated catalyst layers, indicating that there was likely ionomer migration to the surface during drying of the rod-coated samples. This also suggests that forming the catalyst layer from a thick wet film – as opposed to many sequential very thin layers, as is the case in spray coating – may provide an advantage for preparing GDEs. With increasing I/C from 0.9 to 1.2 and 1.6 there is an increase in CPD regardless of drying temperature, which is expected due to the increased ionomer content of the catalyst layer. There is also an increase in CPD with increasing drying temperature. Increasing the drying temperature increases the evaporation rate and thus *Pe*. Previous studies have shown that high *Pe* favors the segregation of small particles to the top surface of the wet film as it dries [20–22]. In catalyst inks, the ionomer should be the smaller particle as its size has been shown to be in range of 10s–~200 nm [44–51], whereas the primary catalyst aggregate is several hundred nanometers with secondary agglomerates over a micron [52]. Thus it is consistent with prior work that higher *Pe* (higher temperature) favors an increase in the ionomer surface concentration.

To confirm the results of the Kelvin probe measurements we also measured selected GDEs using XPS. Like Kelvin probe, XPS is a surface-specific measurement, but is more quantitative because the ratios of different elements and/or specific species can be compared, either from comparison of the peaks arising from different elements, or from curve-fitting the peak corresponding to a given element. For these GDEs, quantitative information about the relative abundance of ionomer and catalyst at the surface of the catalyst layer was estimated from C 1s spectra, by comparing the contributions from carbon associated with ionomer and carbon present in the catalyst support [40]. The area for the ionomer is the sum of the area of the CF_2 and O-CF_2 peaks (denoted as C_I). The area corresponding to species present in the Pt/HSC catalyst is the sum of the area of the C═C and C–C-/C–H peaks (denoted as C_C). Because these peaks are separated by such a large value (approximately 6 eV) we are able to clearly resolve the peaks for both components in a consistent manner.

Fig. 3 shows the C 1s spectra for the rod-coated GDEs dried at 80 °C as well as spray-coated GDEs with and without an ionomer overlayer. The ratio of ionomer peak area (C_I) to Pt/HSC peak area (C_C) are reported in Table 1. The ratios are calculated such that higher values indicate an increase in surface ionomer content. With increasing I/C ratio we see an increase in the C_I/C_C ratio corresponding to an increase in surface ionomer content, consistent with the Kelvin probe measurements. We observe that all rod-coated GDEs have a larger peak area ratio than the spray-coated GDE without overlayer, which is also consistent with Kelvin probe. When we add the ionomer overlayer to spray-coated GDE we observe an increase in the surface ionomer content. However, the increase is smaller than expected when compared to the rod-coated GDEs. From the Kelvin probe data, the spray-coated GDE with an overlayer has a CPD that is over 100 mV higher than the rod-coated GDE with 1.6 I/C dried at 80 °C. In contrast, the XPS peak area ratio of the spray-coated GDE with an overlayer is less than half of the rod-coated GDE with 1.6 I/C dried at 80 °C. We do not fully understand the source of this inconsistency. It may come from the difference in the two measurement techniques. XPS measures the top 5–10 nm of a sample. Kelvin probe, in theory, should measure only the surface. Thus, we may be seeing a difference due to XPS probing to a deeper depth than Kelvin probe. Despite this relative inconsistency in the two measurements, as a whole the XPS and Kelvin probe Results both indicate that increasing drying temperature and I/C lead to an increase in surface ionomer concentration for the rod-coated GDEs.

From these Results it is clear that drying was influencing the distribution of ionomer in the catalyst layers. However, Kelvin probe and XPS are surface sensitive techniques, and thus do not provide information about the ionomer distribution through the thickness of the catalyst layer. Therefore, we have also examined a select set of rod-coated electrodes using nano-CT to gain more information about the 3D microstructure of the catalyst layers. Nano-CT is a powerful tool to characterize the three-dimensional secondary pore structure in the catalyst layers. Additionally, by exchanging sulfonic groups in the PFSA ionomer with Cs^+, the ionomer distribution throughout the catalyst layer sample can be estimated by correlating X-ray absorption intensity with ionomer volume fraction. Thus it provides a more complete picture of catalyst layer morphology [38,53–55].

Shown in Fig. 4a is the absorption contrast image of the 0.9 I/C rod-coated GDE dried at 80 °C. The absorption contrast data highlights X-ray attenuation from Cs^+ in the sample and shows the distribution of ionomer with blue indicating a lower amount of ionomer and green/yellow indicating a high ionomer concentration. Looking at this image one can see the catalyst layer is mostly blue near the bottom (near the GDM) and becomes much greener moving towards the top. This shows that the ionomer concentration is increasing towards the top of the catalyst layer.

To more clearly characterize the distribution of ionomer, the ionomer volume fraction is presented along the electrode thickness in Fig. 4b. Here the thickness has been normalized by the total layer thickness with 0 corresponding to the top (air) surface and 1 corresponding to the interface with the GDM. Overall, the trends are consistent with the Results of Kelvin probe and XPS. Comparing the 1.6 I/C inks dried at 25 and 80 °C, focusing on the air surface (left side) of the profile, we do see that the catalyst layer dried at 80 °C has a higher ionomer content. This is consistent with what was measured with the Kelvin probe. Also compared is the effect of I/C. Consistent with the Kelvin probe and XPS, increasing I/C leads to an increase the surface concentration of ionomer.

If we look at the whole thickness profile, we can see that none of the catalyst layers show complete stratification of ionomer and Pt/HSC into a bilayer structure that has been observed for some particle systems and conditions [20,21]. Rather the profiles are gradients with ionomer content gradually increasing towards the surface. These profiles look similar to the results of Makepeace et al. for concentrated dispersions with a small size ratio between large and small particles, suggesting the

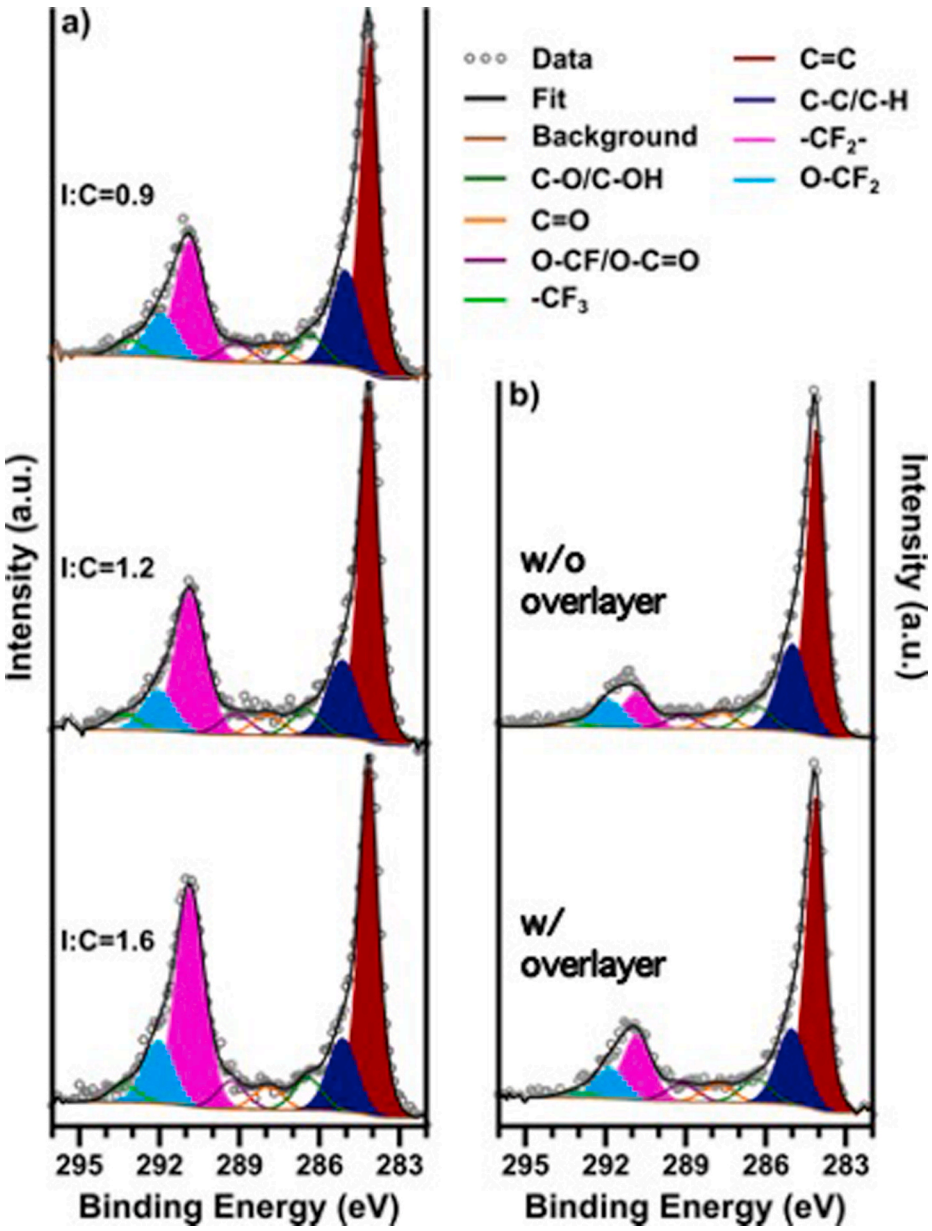


Fig. 3. C 1s XPS spectra for GDEs coated on 29BC diffusion media. (a) Rod-coated GDEs as a function of catalyst ink I/C, increasing from top to bottom. (b) Spray-coated GDEs without (top) and with (bottom) an ionomer overlayer. *Ionomer signal area is calculated as the sum of the areas for the -CF2- (pink) and -O-CF_2- (cyan) peaks (C_I). The total catalyst area is calculated as the sum of the areas for the C = C (red) and C–C/C–H (dark blue) peaks (C_C).* (For interpretation of the references to colour in this figure legend, the reader is referred to the Web version of this article.)

Table 1
Summary of XPS measurements of rod-coated and spray-coated GDEs dried at 80 °C. The C_I/C_C ratio is the peak area ratio of peaks unique to the ionomer (C_I) and Pt/HSC catalyst (C_C). Also included are the relative CPD difference between the samples and the spray-coated GDE without an overlayer.

Coating Method	I/C	C_I/C_C	ΔCPD [mV]
Spray-coated without overlayer	0.9	0.21	–
Spray-coated with overlayer	0.9	0.38	1104
Mayer Rod	0.9	0.49	605
	1.2	0.58	726
	1.6	0.86	933

same conditions may exist here for the ink formulations used [20]. From our previous DLS measurements of particles sizes we have measured Pt/HSC primary aggregates to be 298 nm and ionomer aggregates to be around 200 nm [56,57]. This gives an estimated size ratio of 1.5, consistent with the low size ratio studied by Makepeace et al. Based on small angle neutron measurements of carbon blacks [58], we estimate that the effective volume fraction of HSC in the inks used here is around 0.15. With the additional volume fraction of the ionomer this is close to the 0.2 vol fraction considered as concentrated by Makepeace et al. Ultimately these results and analysis confirm that our observations of the stratification during consolidation for this ink is consistent with general studies of drying in colloidal mixtures.

From Kelvin probe, XPS, and nano-CT it is clear that increasing drying temperature increases the surface ionomer content. This would indicate that the drying of these catalyst layers at high temperatures is dominated by evaporative forces. A rough estimate of *Pe* confirms this. At 80 °C the films were dry in less than 1 min. The wet film thickness (H_0) for a 0.1 mg_{Pt}/cm^2 loading is approximately 60 μm. This Results in an evaporation rate (E) of 1 μm/s. Assuming a particle diameter of 300 nm and a viscosity of 100 mPa-s, D_0 is on the order of 10^{-14} m^2/s. From Eqn. (1), we estimate that *Pe* is on the order of 10^3, indicating that film consolidation is evaporation dominated at 80 °C.

In addition to characterizing the ionomer volume fraction, the nano-CT measurements can be used to estimate the local ion conductivity and oxygen diffusivity, as shown in Fig. 4c and d, respectively. The calculations of local ion conductivity and oxygen diffusivity are consistent

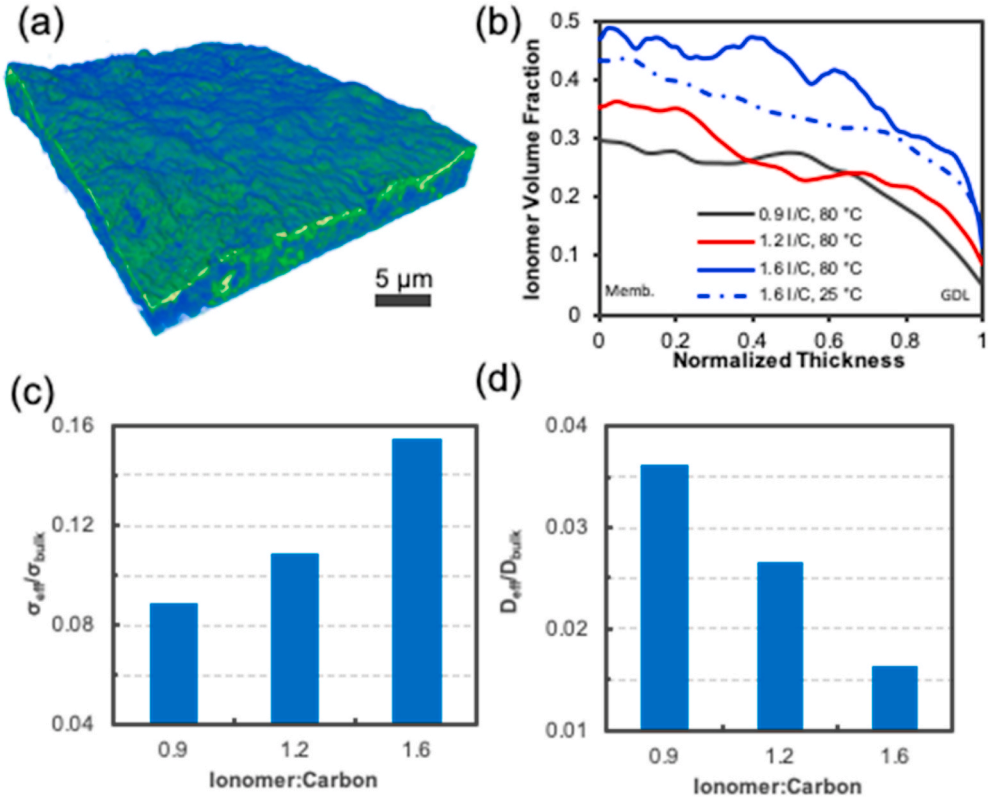


Fig. 4. (a) Example of absorption contrast data showing Cs^+ intensity (blue: low, green: high intensity) (b) Spatial distribution of ionomer volume fraction (c) Effective cation conductivity and (d) effective oxygen modeled from the 3D reconstructions. (For interpretation of the references to colour in this figure legend, the reader is referred to the Web version of this article.)

with what would be expected with increases in I/C. The effective proton conductivity increases with increasing I/C, which would be expected based on the increased volume fraction of ionomer in the catalyst layer [59]. Similarly, increasing I/C decreases the effective oxygen diffusivity. From the pore size distributions of the phase contrast images, increasing I/C decreases the average porosity, which leads to lower diffusivity. We also found that decreasing the drying temperature decreases the average porosity. At lower drying temperatures, thus lower *Pe,* greater diffusional motion should allow the Pt/HSC aggregates to pack more closely, reducing the secondary pore diameter.

Based on the Results from the Kelvin probe, XPS, and nano-CT measurements, we concluded that there could be advantages to preparing GDEs from thick wet films as compared to spray coating due to the higher surface ionomer concentration. Therefore, we prepared R2R slot-die-coated GDEs using the same ink formulations that were used for the rod-coated samples. Slot-die coating is a pre-metered liquid coating technique suitable for continuous R2R coating [60,61]. Line speeds of over 100 m/min are possible, which is well above the estimated requisite line speeds for industrial fuel cell manufacturing [1,61]. Previous researchers have demonstrated the capability of slot-die coating to fabricate highly uniform fuel cell catalyst layers [62,63]. In slot-die coating, the coating liquid is fed to the die body and extruded through a thin slot directly onto the substrate. Because slot-die coating is a non-contact coating method it enables uniform liquid film coatings on rough or irregular surfaces, such as GDM [64]. The drying temperature for these fabrications was set at 80 °C, as we observed higher drying temperature to increase the ionomer content of the top surface.

In our previous work on spray-coated GDEs we found that MPL surface roughness influenced the thickness of the ionomer overlayer needed to achieve best performance [19]. In that work it was shown that, of the two gas diffusion media studied, Freudenberg H23C8 had a relatively smooth MPL surface. And given that our goal in this work was to prepare high-performance GDEs *without* an overlayer, we presumed that this smooth MPL would be advantageous. Therefore, we R2R coated the catalyst layers on Freudenberg H23C8 GDM in addition to the SGL 29BC GDM. These GDEs were assembled into MEAs by hot pressing the GDEs to anode half-CCMs. The 29BC-based R2R-coated GDEs showed very poor fuel cell performance, likely due to the rough MPL surface, and were not analyzed further.

As was done with the rod-coated catalyst layers, we characterized the surface ionomer content of the R2R-coated H23C8-GDM-based GDEs using XPS. These Results are shown in Fig. 5 and summarized in Table 2. We observe the same trend in the R2R-coated GDEs as was observed for the rod-coated GDEs. The R2R-coated GDEs show an increased peak area ratio compared to the spray-coated GDEs, indicating a higher surface ionomer concentration. Additionally, the peak area ratio increases with increasing I/C ratio. R2R-coated GDEs on H23C8 GDM have a much higher C_I/C_C ratio than the rod-coated GDEs on 29BC GDM. At this point we are unsure of the cause of these differences. It is possible that the difference in surface roughness effects the measured signal. It may also be that the substrate or coating method may additionally be affecting the distribution of ionomer. Further investigation is needed to determine the cause(s). Regardless, the results are qualitatively consistent and confirm that drying from a thick liquid film leads to an enrichment of ionomer on the top surface of the catalyst layer.

Finally, we prepared MEAs from the R2R-coated GDEs as well as spray-coated GDEs using the same H23C8 GDM. The oxygen polarization curves are presented in Fig. 6. The ECSA (measured from cyclic voltammetry) and oxygen-reduction reaction (ORR) mass activity (measured at 0.9 V HFR-free) are reported for all MEAs in Table 3. All of the MEAs show very similar ECSA, consistent with our previous Results that showed ECSA was not significantly impacted by the catalyst layer-membrane interface so long as the GDEs were hot pressed to the membrane [18]. The R2R-coated GDEs display very similar mass activity to

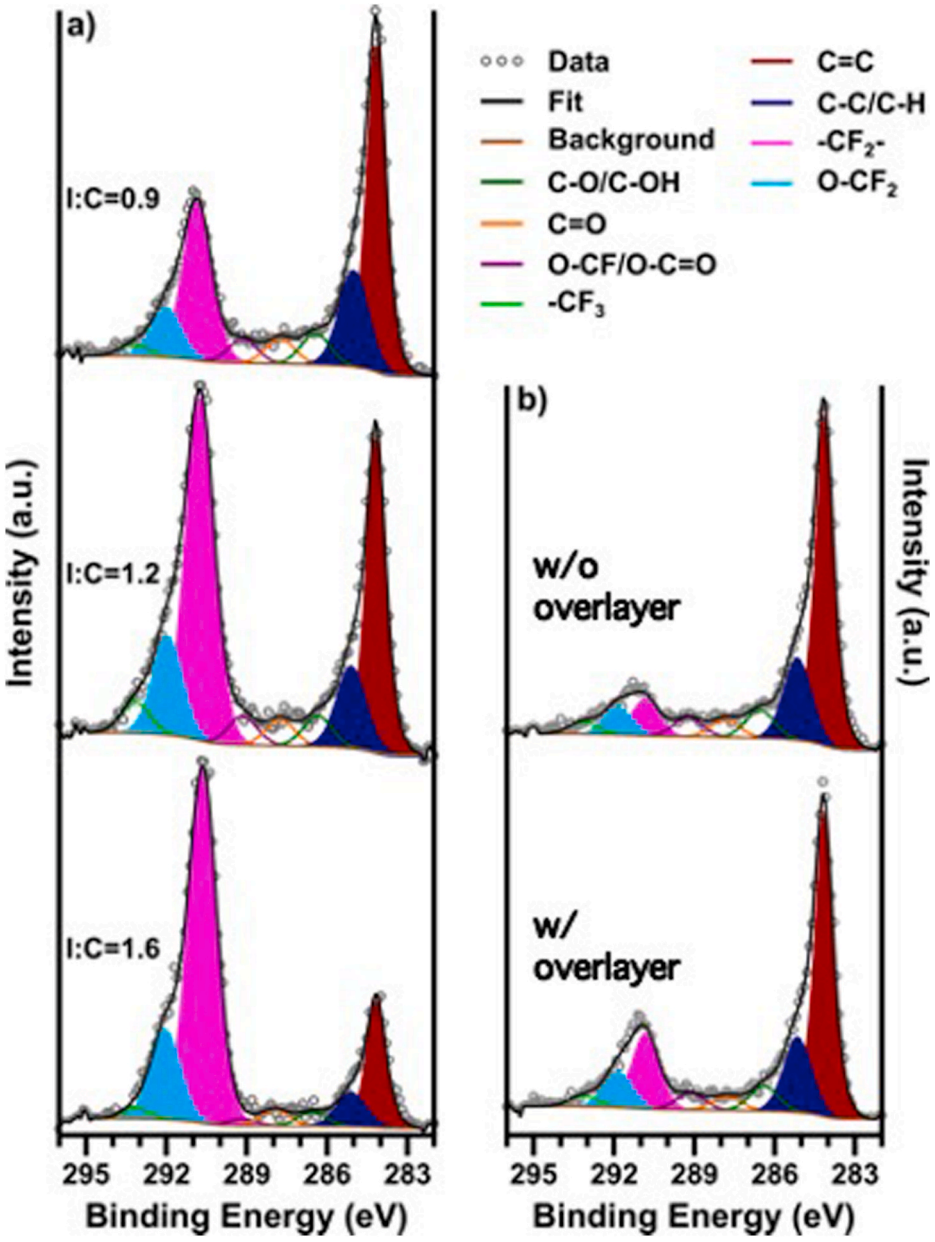


Fig. 5. C 1s XPS spectra for GDEs coated on H23C8 diffusion media. (a) Slot-die-coated GDEs as a function of catalyst ink I/C, increasing from top to bottom. (b) Spray coated GDEs without (top) and with (bottom) an ionomer overlayer. *Ionomer signal area is calculated at the sum of the areas for the -CF2- (magenta) and -O-CF_2- (cyan) peaks. The total catalyst area is calculated as the sum of the areas for the C = C (red) and C–C/C–H (dark blue) peaks.* (For interpretation of the references to colour in this figure legend, the reader is referred to the Web version of this article.)

Table 2
XPS analysis of R2R-coated GDEs coated on H23C8 diffusion media. The peak areas are reported for the C 1s peaks associated with carbon in ionomer (C_I) and catalyst support (C_S). Higher values of C_I/C_S indicate a greater surface ionomer concentration.

Coating Method	I/C	C_I/C_S
Spray – no overlayer	0.9	0.21
Spray – overlayer	0.9	0.38
R2R slot die	0.9	0.63
	1.2	1.4
	1.6	3.6

the spray-coated GDEs with an overlayer indicating similar Pt utilization and ORR kinetics.

Fig. 7a shows the H_2/air polarization curves at 100 %RH for the R2R MEAs. Additional polarization curve details are reported in Table S2. It can be seen that the spray-coated GDE without an overlayer performs poorly compared to the spray-coated GDE with an overlayer, as we have demonstrated previously [18,19]. The spray-coated GDE with the overlayer was also shown to perform better than CCMs with this diffusion media [19]. The one-step (without an overlayer) R2R GDE with a 0.9 I/C performs slightly better than the spray-coated GDE with an ionomer overlayer, e.g., at 1.5 A/cm^2 the cell voltage of the R2R-coated GDE is 23 mV higher than that of the spray-coated GDE with overlayer. This difference in cell voltage is greater than the standard deviation measured for multiple MEAs indicating that this difference is real and not a result of experimental variance.

As we observed in the Kelvin probe, XPS, and nano-CT measurements, the GDEs coated from thick liquid films (rod and slot die) resulted in higher surface ionomer content than spray coating. We suspected that this behavior could lead to the formation of an interface with the membrane upon hot pressing sufficient to eliminate the need for an ionomer overlayer. The similar ECSA, mass activity, and air performance of the R2R-coated GDEs (without a sprayed overlayer) compared to the spray-coated GDEs with an overlayer confirm this hypothesis.

Interestingly, the higher measured surface ionomer content of the 1.2 and 1.6 I/C GDEs does not result in any improvement in performance

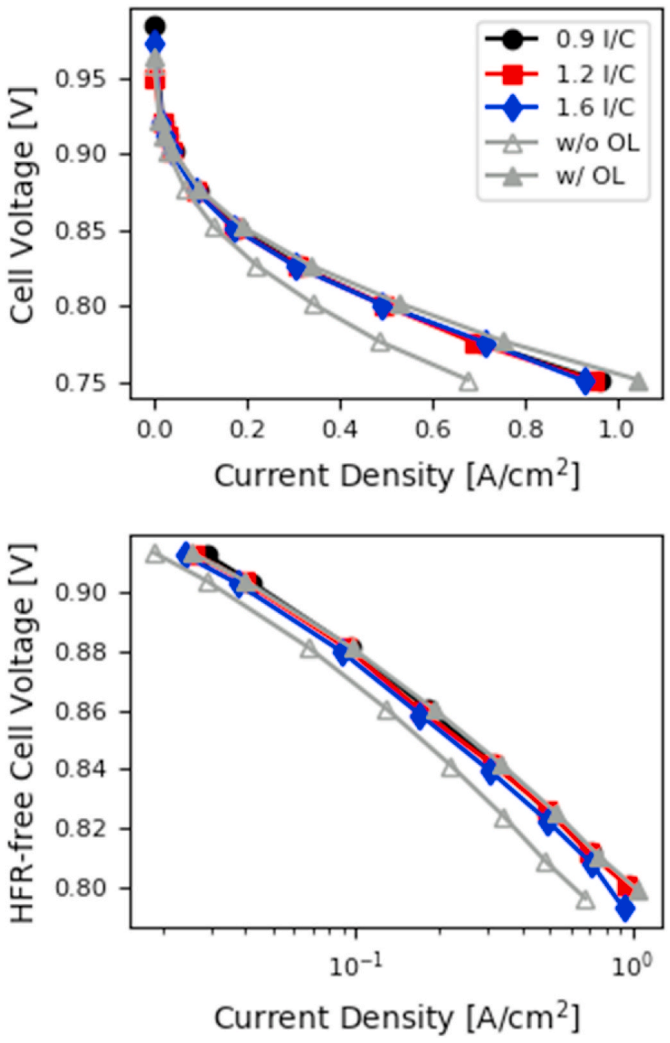


Fig. 6. Oxygen polarization curves for MEAs with R2R-coated and spray-coated cathode GDEs. (a) Current density vs. cell voltage. (b) Current density vs. HFR-free cell voltage.

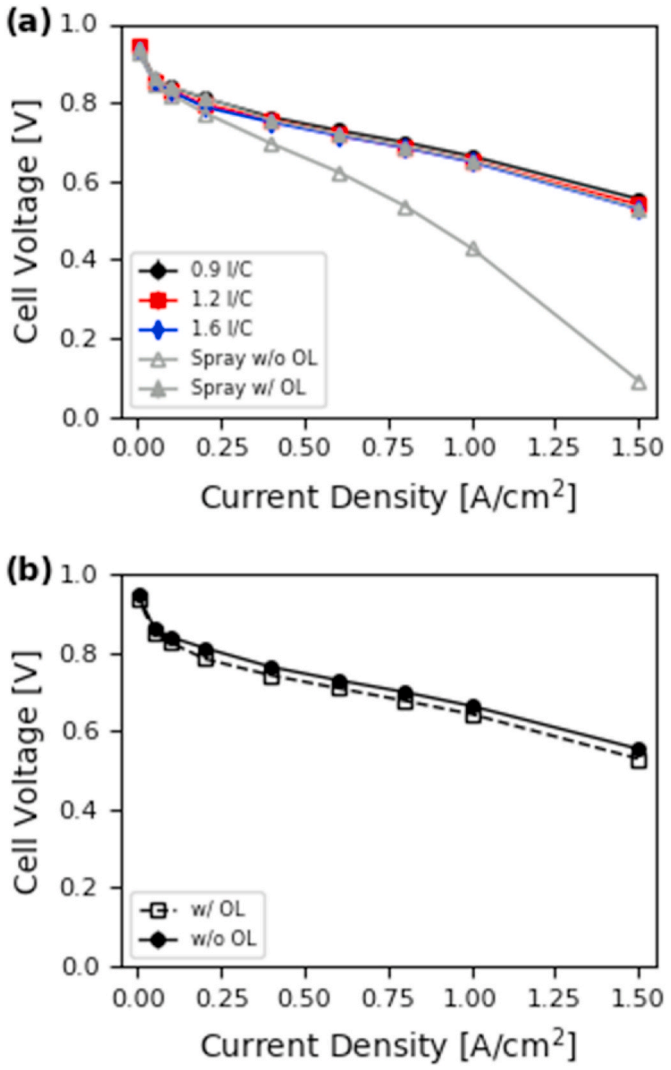


Fig. 7. (a) Air polarization curves for MEAs with R2R-coated and spray-coated cathode GDEs. The spray-coated GDEs were prepared with an 0.023 mg_{Naf}/cm^2 ionomer overlayer (w/OL) or without an overlayer (w/o OL) (These data were previously reported in Ref. [19].) (b) Comparison of R2R-coated GDEs with 0.9 I/C prepared with 0.023 mg_{Naf}/cm^2 ionomer overlayer (w/OL) or without an overlayer (w/o OL). Polarization curves were measured at 80 °C, 100 %RH, and 150 $kPa_{abs.}$

Table 3
Electrochemical surface area (ECSA) and ORR mass activity ($i_m^{0.9V}$) for MEAs prepared with R2R-coated and spray-coated GDEs.

Coating Method	I/C	ECSA [m^2/g]	$i_m^{0.9V}$ [mA/mg_{Pt}]
Roll-to-Roll	0.9	61.5 ± 2.0	392 ± 12
	1.2	60.9 ± 3.1	387 ± 10
	1.6	58.5 ± 4.2	367 ± 15
Spray – without ionomer overlayer[a]	0.9	59.8	317 ± 8
Spray – with ionomer overlayer[a]	0.9	62.9 ± 3.5	427 ± 16

[a] Data previously published in Reference [19].

over the GDEs at 0.9 I/C. In fact, these samples show slightly decreased performance compared to 0.9 I/C. There is also a slight decrease in performance at high current density as well as small decreases in both ECSA and mass activity (Table S2) with increasing I/C, but all of these deviations are small and may be within experimental error. These findings indicate that the additional surface ionomer in the 1.2 and 1.6 I/C R2R GDEs beyond what is present in the 0.9 I/C R2R GDE is not necessary to form a good interface with the membrane and may be leading to electrically-isolated catalyst aggregates. Also, the lower effective oxygen diffusivities shown in Fig. 4d indicate the additional ionomer could be limiting transport within these catalyst layers and diminishing the performance.

To confirm that the 0.9 I/C GDE has sufficient surface ionomer for maximized performance, we sprayed an ionomer overlayer onto a 0.9 I/C R2R GDE and assembled it into an MEA. The air polarization curves for 0.9 I/C R2R GDEs with and without an ionomer overlayer are shown in Fig. 7b. It is clearly seen that the overlayer does not improve the fuel cell performance. This offers further confirmation that the surface ionomer concentration of the 0.9 I/C R2R GDE does not need further enrichment to achieve good performance.

To further understand the influence of the surface ionomer concentration of the R2R-coated GDEs on MEA performance, we compared these MEAs using H_2/N_2 electrochemical impedance spectroscopy (EIS). The impedance spectra were fit using a physics-based impedance model [18,32,33]. The Bode plots of the impedance magnitude (|Z|) with the model fits for the entire frequency are shown in Figure S1 of the supporting information to show the quality of the fit. The model fit parameter values are also reported in Table S3. The Nyquist plots of measured impedance spectra with the model fits are shown in Fig. 8a. . The fitted values of the catalyst layer protonic sheet resistance [59] (R_{CL})

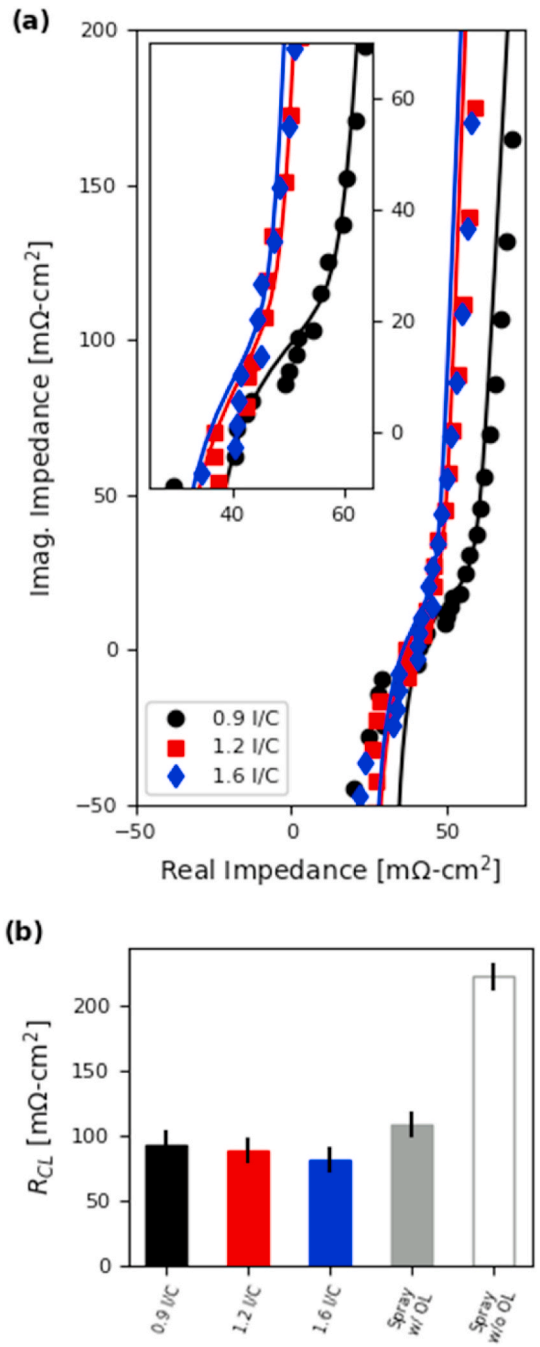


Fig. 8. (a) H_2/N_2 impedance spectra for R2R-coated GDEs. Lines shows the fits of the physics-based model of the measured data. The inset figure shows a smaller segment of the spectra to more clearly show the region of the spectra where R_{CL} (b) Values of R_{CL} obtained from fitting of the physics-based model to measured spectra. All spectra were measured at 80 °C, 100 %RH, 150 kPa_{abs}. Values for spray-coated GDEs from Ref. [19].

Table 4
Summary of R_{CL} values obtained from fitting of H_2/N_2 impedance spectra. Values for spray-coated GDEs from Ref. [19].

Coating Method	I/C	R_{CL} [mΩ-cm²]
Roll-to-Roll	0.9	92 ± 10
	1.2	88 ± 10
	1.6	81 ± 10
Spray – without ionomer overlayer	0.9	222 ± 10
Spray – with ionomer overlayer	0.9	108 ± 10

are reported in Table 4 and shown in Fig. 8b, with a comparison to spray-coated GDEs from our previous work [19]. The inset plot in Fig. 8a shows smaller portion of the spectra to more clearly show the region where R_{CL} predominates. We previously found that for GDE-based MEAs, R_{CL} is comprised of both the bulk catalyst layer resistance and the catalyst layer – membrane interfacial resistance [18]. We also observed that spray-coated GDEs without an ionomer overlayer had a significantly higher R_{CL} than those with an overlayer due to a poor interface between the membrane and the catalyst layer.

For all the R2R-coated GDEs, the measured R_{CL} values are similar, though there is a slight decrease with increasing I/C. Also, all are slightly lower than those measured for the spray-coated GDEs with an ionomer overlayer. Overall, this is consistent with the similarity of the polarization curves for the spray-coated GDE with an overlayer and the R2R-coated GDEs and offers further confirmation that the higher surface ionomer content of the R2R-coated GDEs is sufficient to form a good interface with the membrane. Interestingly, even though increasing I/C in the R2R-coated GDEs leads to a slight decrease in the mean R_{CL} it does not lead to an increase in electrochemical performance. Since the 0.9 I/C R2R-coated GDE has a lower R_{CL} than the spray-coated GDE with an overlayer it indicates the 0.9 I/C R2R-coated GDE has sufficient surface ionomer concentration to form a good interface with the membrane, thus adding additional ionomer by increasing I/C offers no measurable benefit to MEA performance as it does not further improve the catalyst layer – membrane interface. Instead of decreasing the interfacial resistance, it is likely that the small decrease in R_{CL} with increasing I/C is due to the increase in effective proton conductivity shown in Fig. 4c leading to a decrease in the bulk proton resistance of the catalyst layer. As was discussed previously, the additional ionomer above 0.9 I/C is overall negatively impacting cell performance, which is likely due to the additional ionomer altering other properties of the catalyst layer. As shown in Fig. 4d, the additional I/C Results in lower oxygen diffusivity due to it filling more of the catalyst layer pore space, which likely explains the decreased cell voltage at high current density (see cell voltage data 1.5 A/cm² in Table S2). It seems that this effect outweighs any potential benefits from the decreased R_{CL}.

4. Conclusions

In this study we have demonstrated a one-step coating process for the fabrication of high performance R2R-coated GDEs. The Results show the importance of understanding the distribution of ionomer and catalyst in R2R-coated catalyst layers as they are critical for maximizing fuel cell performance. These results also highlight the importance of understanding how the coating and drying parameters influence the distribution of materials in a catalyst layer, which, as we have shown here, can have significant impacts on performance. Using spray coating, the total thickness of the catalyst layer is formed by coating many thin layers. Such a methodology does not allow for designed segregation of ionomer. In contrast, when the catalyst layer is coated as a thick liquid film (e.g., by rod or slot die) with high *Pe* drying, the high evaporation rate leads to an enrichment of ionomer at the top surface of the dry film, as shown by Kelvin probe, XPS, and nano-CT. This enrichment is beneficial for creating higher performance GDE-based MEAs by enabling the formation of a low-resistance interface between the catalyst layer and membrane. Furthermore, due to this enrichment we are able to fabricate high-performance GDE-based MEAs without the ionomer overlayer that is needed for spray-coated GDEs. This is a significant advantage for large-scale manufacturing of fuel cells because it eliminates a process step, simplifying manufacturing and reducing process costs. This also shows that when designing fuel cell components, the manufacturing process needs to be considered as it may impact the properties and performance of the component. Thus, various processing parameters such as ink formulation, drying temperature, air flow rate, etc. must be considered in parallel with materials selection to obtain a fuel cells that meet the required specifications.

CRediT authorship contribution statement

Scott A. Mauger: Conceptualization, Investigation, Writing – original draft, Visualization, Formal analysis. **Min Wang:** Investigation, Writing – review & editing, Formal analysis. **Firat C. Cetinbas:** Investigation, Visualization, Formal analysis, Resources. **Michael J. Dzara:** Investigation, Visualization, Formal analysis. **Jaehyung Park:** Resources, Investigation. **Deborah J. Myers:** Resources, Investigation, Supervision. **Rajesh K. Ahluwalia:** Writing – review & editing. **Svitlana Pylypenko:** Supervision, Writing – review & editing. **Leiming Hu:** Resources. **Shawn Litster:** Supervision. **K.C. Neyerlin:** Conceptualization, Supervision, Writing – review & editing. **Michael Ulsh:** Conceptualization, Project administration, Funding acquisition, Writing – review & editing.

Declaration of competing interest

The authors declare that they have no known competing financial interests or personal relationships that could have appeared to influence the work reported in this paper.

Acknowledgements

This work was authored in part by the National Renewable Energy Laboratory, operated by Alliance for Sustainable Energy, LLC, for the U. S. Department of Energy (DOE) under Contract No. DE-AC36-08GO28308. The submitted manuscript was created, in part, by U Chicago Argonne, LLC, Operator of Argonne National Laboratory, Argonne, U.S. Department of Energy Office of Science laboratory, operated under Contract No. DE-AC02-06CH11357. This research used the resources of the Advanced Photon Source (APS), a U.S. Department of Energy (DOE) Office of Science User Facility, operated for the DOE Office of Science by Argonne National Laboratory, also under Contract No. DE-AC02 06CH11357. Funding provided by U.S. Department of Energy, Office of Energy Efficiency and Renewable Energy, Advanced Manufacturing Office. This work was conducted as part of the Roll-to-Roll Advanced Materials Manufacturing Laboratory Collaboration, and strongly leveraged work supported by the Hydrogen and Fuel Cell Technologies Office. The views expressed in the article do not necessarily represent the views of the DOE or the U.S. Government. MJD and SP acknowledge support from NSF PFI-RP award #1919280-Commercializing Active and Durable Materials and Electrodes for Fuel Cell and Electrolyzer Applications, and from the Colorado Energy Research Collaboratory. This work makes use of the E-XPS system at the Colorado School of Mines, which was supported by the National Science Foundation under Grant No. 1626619.

Appendix A. Supplementary data

Supplementary data to this article can be found online at https://doi.org/10.1016/j.jpowsour.2021.230039.

References

[1] M.K. Debe, Electrocatalyst approaches and challenges for automotive fuel cells, Nature 486 (2012) 43–51, https://doi.org/10.1038/nature11115.
[2] B.D. James, J.M. Huya-Kouadio, C. Houchins, D.A. DeSantis, Mass ProductionCostEstimation of direct H2PEM fuel cell systems for transportation Applications: 2018 update. https://www.energy.gov/sites/prod/files/2019/12/f70/fcto-sa-2018-transportation-fuel-cell-cost-analysis.pdf, 2018.
[3] C. Daniel, S.A. Mauger, Roll-to-Roll advanced materials manufacturing lab collaboration, US DOE hydrog, in: Fuel Cell Program 2018 Annu. Merit Rev. Peer Eval., 2018. https://www.hydrogen.energy.gov/pdfs/review19/ta007_daniel_2019_o.pdf.
[4] M. Prasanna, H.Y. Ha, E.A. Cho, S.A. Hong, I.H. Oh, Investigation of oxygen gain in polymer electrolyte membrane fuel cells, J. Power Sources 137 (2004) 1–8, https://doi.org/10.1016/j.jpowsour.2004.05.034.
[5] C.H. Hsu, C.C. Wan, An innovative process for PEMFC electrodes using the expansion of Nafion film, J. Power Sources 115 (2003) 268–273, https://doi.org/10.1016/S0378-7753(03)00005-3.
[6] I.-S. Park, W. Li, A. Manthiram, Fabrication of catalyst-coated membrane-electrode assemblies by doctor blade method and their performance in fuel cells, J. Power Sources 195 (2010) 7078–7082, https://doi.org/10.1016/j.jpowsour.2010.05.004.
[7] W. Wang, S. Chen, J. Li, W. Wang, Fabrication of catalyst coated membrane with screen printing method in a proton exchange membrane fuel cell, Int. J. Hydrogen Energy 40 (2015) 4649–4658, https://doi.org/10.1016/j.ijhydene.2015.02.027.
[8] S.G. Yan, J.C. Doyle, B. Sompalli, H.A. Gasteiger, J. O'Hara, W. Gu, Control Parameters for Optimizing MEA Performance, US2006/0204831A1, 2006.
[9] R. Baumann, A. Willert, F. Siegel, A. Kohl, Method for producing catalyst layers for fuel cells, US2012/0125211A1. http://www.google.com/patents/US20120125211, 2012.
[10] D.W. Fultz, P.-Y.A. Chuang, The property and performance differences between catalyst coated membrane and catalyst coated diffusion media, J. Fuel Cell Sci. Technol. 8 (2011), 041010, https://doi.org/10.1115/1.4003632.
[11] S. Kim, M. Khandelwal, C. Chacko, M.M. Mench, Investigation of the impact of interfacial delamination on polymer electrolyte fuel cell performance, J. Electrochem. Soc. 156 (2009) B99–B108, https://doi.org/10.1149/1.3006398.
[12] I.V. Zenyuk, E.C. Kumbur, S. Litster, Deterministic contact mechanics model applied to electrode interfaces in polymer electrolyte fuel cells and interfacial water accumulation, J. Power Sources 241 (2013) 379–387, https://doi.org/10.1016/j.jpowsour.2013.03.165.
[13] K. Kadowaki, Y. Tabe, T. Chikahisa, Role of micro-porous layer for water transfer phenomena in PEFC, ECS Trans 41 (2011) 431–438, https://doi.org/10.1149/1.3635577.
[14] J.-H. Kim, H.Y. Ha, I.-H. Oh, S.-A. Hong, H.-I. Lee, Influence of the solvent in anode catalyst ink on the performance of a direct methanol fuel cell, J. Power Sources 135 (2004) 29–35, https://doi.org/10.1016/j.jpowsour.2004.03.058.
[15] S.G. Yan, B. Sompalli, J.C. Doyle, Durable membrane electrode assembly catalyst coated diffusion media with no lamination to membrane, US, 7,291,419 B2, http://www.google.com/patents/US7291419, 2007.
[16] C.-C. Sung, C.-Y. Liu, C.C.J. Cheng, Performance improvement by a glue-functioned Nafion layer coating on gas diffusion electrodes in PEM fuel cells, Int. J. Hydrogen Energy 39 (2014) 11700–11705, https://doi.org/10.1016/j.ijhydene.2014.05.110.
[17] J.-C. Lin, C.-M. Lai, F.-P. Ting, S.-D. Chyou, K.-L. Hsueh, Influence of hot-pressing temperature on the performance of PEMFC and catalytic activity, J. Appl. Electrochem. 39 (2009) 1067–1073, https://doi.org/10.1007/s10800-008-9758-1.
[18] S.A. Mauger, J.R. Pfeilsticker, M. Wang, S. Medina, A.C. Yang-Neyerlin, K. C. Neyerlin, C. Stetson, S. Pylypenko, M. Ulsh, Fabrication of high performance gas-diffusion-electrode based membrane-electrode assemblies, J. Power Sources 450 (2020) 227581, https://doi.org/10.1016/j.jpowsour.2019.227581.
[19] M. Wang, S. Medina, J.R. Pfeilsticker, S. Pylypenko, M. Ulsh, S.A. Mauger, Impact of microporous layer roughness on gas-diffusion-electrode-based polymer electrolyte membrane fuel cell performance, ACS Appl. Energy Mater. 2 (2019) 7757–7761, https://doi.org/10.1021/acsaem.9b01871.
[20] D.K. Makepeace, A. Fortini, A. Markov, P. Locatelli, C. Lindsay, S. Moorhouse, R. Lind, R.P. Sear, J.L. Keddie, Stratification in binary colloidal polymer films: experiment and simulations, Soft Matter 13 (2017) 6969–6980, https://doi.org/10.1039/C7SM01267E.
[21] C.M. Cardinal, Y.D. Jung, K.H. Ahn, L.F. Francis, Drying regime maps for particulate coatings, AIChE J. 56 (2010) 2769–2780, https://doi.org/10.1002/aic.12190.
[22] H. Luo, C.M. Cardinal, L.E. Scriven, L.F. Francis, Ceramic nanoparticle/monodisperse latex coatings, Langmuir 24 (2008) 5552–5561, https://doi.org/10.1021/la800050u.
[23] S. Jaiser, M. Müller, M. Baunach, W. Bauer, P. Scharfer, W. Schabel, Investigation of film solidification and binder migration during drying of Li-Ion battery anodes, J. Power Sources 318 (2016) 210–219.
[24] J.W. Dappen, Distribution of starch in clay coatings, Tappi J. 34 (1951) 324–355.
[25] R. Tatsumi, T. Iwao, O. Koike, Y. Yamaguchi, Y. Tsuji, Effects of the evaporation rate on the segregation in drying bimodal colloidal suspensions, Appl. Phys. Lett. 112 (2018), 053702, https://doi.org/10.1063/1.5013194.
[26] S. Baesch, K. Price, P. Scharfer, L. Francis, W. Schabel, Influence of the drying conditions on the particle distribution in particle filled polymer films: experimental validation of predictive drying regime maps, Chem. Eng. Process. - Process Intensif. 123 (2018) 138–147, https://doi.org/10.1016/j.cep.2017.10.018.
[27] S. Lim, K.H. Ahn, M. Yamamura, Latex migration in battery slurries during drying, Langmuir 29 (2013) 8233–8244, https://doi.org/10.1021/la4013685.
[28] P.A. Rapaport, A.J. Blowers, L. James, B. Lakshmanan, Fast MEA break-in and voltage recovery, US9,099,703B2. http://www.google.com/patents/US9099703, 2015.
[29] S. Kabir, D.J. Myers, N. Kariuki, J. Park, G. Wang, A. Baker, N. Macauley, R. Mukundan, K.L. More, K.C. Neyerlin, Elucidating the dynamic nature of fuel cell electrodes as a function of conditioning: an ex situ material characterization and in situ electrochemical diagnostic study, ACS Appl. Mater. Interfaces 11 (2019) 45016–45030, https://doi.org/10.1021/acsami.9b11365.
[30] D.A. Stevens, J.R. Dahn, Electrochemical characterization of the active surface in carbon-supported platinum electrocatalysts for PEM fuel cells, J. Electrochem. Soc. 150 (2003) A770, https://doi.org/10.1149/1.1573195.
[31] R.N. Carter, S.S. Kocha, F. Wagner, M. Fay, H.A. Gasteiger, Artifacts in measuring electrode catalyst area of fuel cells through cyclic voltammetry, ECS Trans 11 (2007) 403, https://doi.org/10.1149/1.2780954.

[32] B.P. Setzler, T.F. Fuller, A physics-based impedance model of proton exchange membrane fuel cells exhibiting low-frequency inductive loops, J. Electrochem. Soc. 162 (2015) F519–F530, https://doi.org/10.1149/2.0361506jes.
[33] J.R. Pfeilsticker, Open-source impedance fitter. https://github.com/NREL/OSIF, 2019.
[34] L. Osmieri, S. Mauger, M. Ulsh, K.C. Neyerlin, G. Bender, Use of a segmented cell for the combinatorial development of platinum group metal-free electrodes for polymer electrolyte fuel cells, J. Power Sources 452 (2020) 227829, https://doi.org/10.1016/j.jpowsour.2020.227829.
[35] S. Komini Babu, H.T. Chung, P. Zelenay, S. Litster, Resolving electrode morphology's impact on platinum group metal-free cathode performance using nano-CT of 3D hierarchical pore and ionomer distribution, ACS Appl. Mater. Interfaces 8 (2016) 32764–32777, https://doi.org/10.1021/acsami.6b08844.
[36] D.M. Pelt, D. Gürsoy, W.J. Palenstijn, J. Sijbers, F. De Carlo, K.J. Batenburg, Integration of TomoPy and the ASTRA toolbox for advanced processing and reconstruction of tomographic synchrotron data, J. Synchrotron Radiat. 23 (2016) 842–849, https://doi.org/10.1107/S1600577516005658.
[37] J. Schindelin, I. Arganda-Carreras, E. Frise, V. Kaynig, M. Longair, T. Pietzsch, S. Preibisch, C. Rueden, S. Saalfeld, B. Schmid, J.-Y. Tinevez, D.J. White, V. Hartenstein, K. Eliceiri, P. Tomancak, A. Cardona, Fiji: an open-source platform for biological-image analysis, Nat. Methods 9 (2012) 676–682, https://doi.org/10.1038/nmeth.2019.
[38] F.C. Cetinbas, R.K. Ahluwalia, N.N. Kariuki, D.J. Myers, Agglomerates in polymer electrolyte fuel cell electrodes: Part I. Structural characterization, J. Electrochem. Soc. 165 (2018) F1051–F1058, https://doi.org/10.1149/2.0301813jes.
[39] M.O.M. Edwards, P.G. Karlsson, S.K. Eriksson, M. Hahlin, H. Siegbahn, H. Rensmo, J.M. Kahk, I.J. Villar-Garcia, D.J. Payne, J. Åhlund, Increased photoelectron transmission in High-pressure photoelectron spectrometers using "swift acceleration, Nucl. Instrum. Methods Phys. Res. Sect. Accel. Spectrometers Detect. Assoc. Equip. 785 (2015) 191–196, https://doi.org/10.1016/j.nima.2015.02.047.
[40] K. Artyushkova, M.J. Workman, I. Matanovic, M.J. Dzara, C. Ngo, S. Pylypenko, A. Serov, P. Atanassov, Role of surface Chemistry on catalyst/ionomer interactions for transition metal–nitrogen–carbon electrocatalysts, ACS Appl. Energy Mater. 1 (2018) 68–77, https://doi.org/10.1021/acsaem.7b00002.
[41] G. Beamson, D. Briggs, High Resolution XPS of Organic Polymers: the Scienta ESCA300 Database, American Chemical Society, 1993, https://doi.org/10.1021/ed070pA25.5.
[42] Y. Liu, C. Ji, W. Gu, J. Jorne, H.A. Gasteiger, Effects of catalyst carbon support on proton conduction and cathode performance in PEM fuel cells, J. Electrochem. Soc. 158 (2011) B614, https://doi.org/10.1149/1.3562945.
[43] S.A. Mauger, M.P. Glasser, B.J. Tremolet de Villers, V.V. Duong, A.L. Ayzner, D. C. Olson, Doped interlayers for improved selectivity in bulk heterojunction organic photovoltaic devices, Adv. Mater. Interfaces. 3 (2015), https://doi.org/10.1002/admi.201500346 n/a-n/a.
[44] T.T. Ngo, T.L. Yu, H.-L. Lin, Influence of the composition of isopropyl alcohol/water mixture solvents in catalyst ink solutions on proton exchange membrane fuel cell performance, J. Power Sources 225 (2013) 293–303, https://doi.org/10.1016/j.jpowsour.2012.10.055.
[45] C. Welch, A. Labouriau, R. Hjelm, B. Orler, C. Johnston, Y.S. Kim, Nafion in dilute solvent systems: dispersion or solution? ACS Macro Lett. 1 (2012) 1403–1407, https://doi.org/10.1021/mz3005204.
[46] G. Gebel, B. Loppinet, Colloidal structure of ionomer solutions in polar solvents, J. Mol. Struct. 383 (1996) 43–49, https://doi.org/10.1016/S0022-2860(96)09266-6.
[47] A. Tarokh, K. Karan, S. Ponnurangam, Atomistic MD study of nafion dispersions: role of solvent and counterion in the aggregate structure, ionic clustering, and acid dissociation, Macromolecules 53 (2020) 288–301, https://doi.org/10.1021/acs.macromol.9b01663.
[48] F. Xu, H. Zhang, J. Ilavsky, L. Stanciu, D. Ho, M.J. Justice, H.I. Petrache, J. Xie, Investigation of a catalyst ink dispersion using both ultra-small-angle X-ray scattering and cryogenic TEM, Langmuir 26 (2010) 19199–19208, https://doi.org/10.1021/la1028228.
[49] B. Loppinet, G. Gebel, C.E. Williams, Small-angle scattering study of perfluorosulfonated ionomer solutions, J. Phys. Chem. B (1997). http://pubs.acs.org/doi/abs/10.1021/jp9623047.
[50] P. Aldebert, B. Dreyfus, M. Pineri, Small-angle neutron scattering of perfluorosulfonated ionomers in solution, Macromolecules 19 (1986) 2651–2653, https://doi.org/10.1021/ma00164a035.
[51] P.J. Dudenas, A. Kusoglu, Evolution of ionomer morphology from dispersion to film: an in situ X-ray study, Macromolecules 52 (2019) 7779–7785, https://doi.org/10.1021/acs.macromol.9b01024.
[52] S. Holdcroft, Fuel cell catalyst layers: a polymer science perspective, Chem. Mater. 26 (2013) 381–393, https://doi.org/10.1021/cm401445h.
[53] F.C. Cetinbas, R.K. Ahluwalia, N. Kariuki, V. De Andrade, D. Fongalland, L. Smith, J. Sharman, P. Ferreira, S. Rasouli, D.J. Myers, Hybrid approach combining multiple characterization techniques and simulations for microstructural analysis of proton exchange membrane fuel cell electrodes, J. Power Sources 344 (2017) 62–73, https://doi.org/10.1016/j.jpowsour.2017.01.104.
[54] F.C. Cetinbas, X. Wang, R.K. Ahluwalia, N.N. Kariuki, R.P. Winarski, Z. Yang, J. Sharman, D.J. Myers, Microstructural analysis and transport resistances of low-platinum-loaded PEFC electrodes, J. Electrochem. Soc. 164 (2017) F1596–F1607, https://doi.org/10.1149/2.1111714jes.
[55] F.C. Cetinbas, R.K. Ahluwalia, Agglomerates in polymer electrolyte fuel cell electrodes: Part II. Transport characterization, J. Electrochem. Soc. 165 (2018) F1059–F1066, https://doi.org/10.1021/ie50355a027.
[56] S. Khandavalli, J.H. Park, N.N. Kariuki, D.J. Myers, J.J. Stickel, K. Hurst, K. C. Neyerlin, M. Ulsh, S.A. Mauger, Rheological investigation on the microstructure of fuel cell catalyst inks, ACS Appl. Mater. Interfaces 10 (2018) 43610–43622, https://doi.org/10.1021/acsami.8b15039.
[57] T. Van Cleve, S. Khandavalli, A. Chowdhury, S. Medina, S. Pylypenko, M. Wang, K. L. More, N.N. Kariuki, D.J. Myers, A.Z. Weber, S. Mauger, M. Ulsh, K.C. Neyerlin, Dictating Pt-based electrocatalyst performance in polymer electrolyte fuel cells; from formulation to application, ACS Appl. Mater. Interfaces 11 (2019) 46953–46964, https://doi.org/10.1021/acsami.9b17614.
[58] J.J. Richards, J.B. Hipp, J.K. Riley, N.J. Wagner, P.D. Butler, Clustering and percolation in suspensions of carbon black, Langmuir 33 (2017) 12260–12266, https://doi.org/10.1021/acs.langmuir.7b02538.
[59] K.C. Neyerlin, W. Gu, J. Jorne, A. Clark, H.A. Gasteiger, Cathode catalyst utilization for the ORR in a PEMFC, J. Electrochem. Soc. 154 (2007) B279, https://doi.org/10.1016/j.jpowsour.2004.03.028.
[60] F. Durst, H.-G. Wagner, Slot coating, in: Liq. Film Coat, Springer Netherlands, Dordrecht, 1997, pp. 401–426, https://doi.org/10.1007/978-94-011-5342-3_11.
[61] X. Ding, J. Liu, T.A.L. Harris, A review of the operating limits in slot die coating processes, AIChE J. 62 (2016) 2508–2524, https://doi.org/10.1002/aic.15268.
[62] A. Burdzik, M. Stähler, I. Friedrich, M. Carmo, D. Stolten, Homogeneity analysis of square meter-sized electrodes for PEM electrolysis and PEM fuel cells, J. Coating Technol. Res. 15 (2018) 1423–1432, https://doi.org/10.1007/s11998-018-0074-3.
[63] M. Bodner, H.R. García, T. Steenberg, C. Terkelsen, S.M. Alfaro, G.S. Avcioglu, A. Vassiliev, S. Primdahl, H.A. Hjuler, Enabling industrial production of electrodes by use of slot-die coating for HT-PEM fuel cells, Int. J. Hydrogen Energy 44 (2019) 12793–12801, https://doi.org/10.1016/j.ijhydene.2018.11.091.
[64] A. Glüsen, M. Müller, D. Stolten, Slot-die coating: a new preparation method for direct methanol fuel cells catalyst layers, J. Fuel Cell Sci. Technol. 10 (2013), 044503.